High Bandwidth Fast Tool Servo Control

Xiaodong Lu and David L. Trumper

***Abstract*— Fast tool servo is one of the key components in manufacturing complex surfaces with nanometer-scale resolution. This paper presents the controller design for an electromagnetically driven fast tool servo. First, the nonlinear and frequency-dependent actuator is linearized with dynamic nonlinear compensation method. Next, the plant is compensated with lead-lag controller plus integrator to achieve the cross over frequency at one twentieth of the sampling frequency. Finally, repetitive controller is plugged into the compensated loop of the last step to improve the tracking of spindle synchronized trajectory and the rejection of spindle rotation induced disturbance. Based on the integrator gain of the compensated loop, a method of tuning repetitive controller gains is presented to ensure the closed loop system phase margin in spite of changes of repetitive controller poles. Experiment is conducted on a diamond turning machine. For 100kHz sampling frequency, the achieved closed loop bandwidth is 10kHz with -3dB attenuation. The maximum stroke is 50um for up to 1kHz operation and the maximum acceleration is 160 g up to 3kHz. An aluminum part is turned with sinusoidal surface to demonstrate the usability of the control.**

***Index Terms*— Fast tool servo, Mechatronics, Feedback linearization, Repetitive control**

I. Introduction

Fast tool servo (FTS) technology can enable precisely manufacturing complicated surfaces with nanometer-scale resolution requirement. Such surfaces are used in a wide range of products, including films for brightness enhancement and controlled reflectivity, as well as in micro-optical devices such as Fresnel lenses and microlens arrays. The limits on stroke, bandwidth, acceleration, and position noise of the FTS impose limits on the types, quality, and rate at which the intended surfaces can be produced. The requirements for high throughput drive simultaneously the need for high bandwidth, high acceleration, and accuracy for the FTS.

Electromagnetic actuators are possible to achieve as high force density as 9105 $\mathrm{N/m^2}$ at 1.5Tesla flux density and thus as high acceleration as 4000 g on a 3mm thick iron disk. As an promising alternative solution to the well-established piezoelectric actuator [1][2][3], the electromagnetically fast tool servo do not have such problems as significant hysteresis loss when materials undergoing deformation and the bandwidth-limiting structural resonance modes of the PZT stacks. Hence the electromagnetically driven fast tool servos are possible to operate at higher frequency than the piezoelectric counterparts.

This project was supported by a 3M Innovation Award to the second author.

The authors are with the Department of Mechanical Engineering, Massachusetts Institute of Technology, MA 02139, USA.

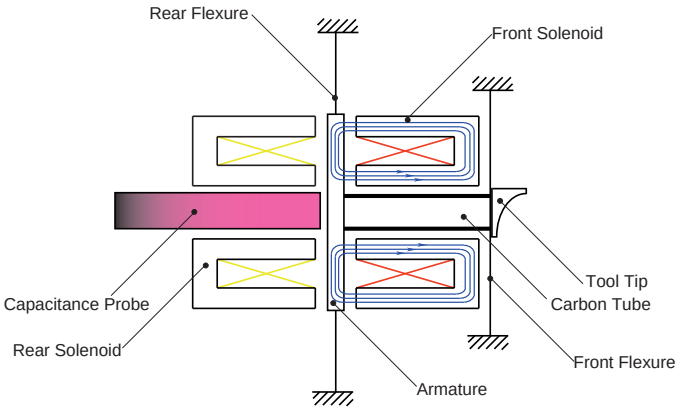

Fig. 1. Electromagnetically driven fast tool servo model.

However, there are several obstacles that limit the performance of the electromagnetically driven fast tool servo. First, the actuating forces nonlinear with air gaps and exciting currents will result in significant tracking errors, which will greatly degrade the tracking performance of fast tool servo. Second, the eddy current induced along the magnetic path will introduce frequency dependent disturbance field and thus further complicate actuator behavior especially at high frequency operation.

On the basis of the static feedback linearization method in [4] , this paper present a dynamic nonlinear compensation method to linearize the actuator. By inverting the actuator operating principle, a feed-forward compensator can be designed to compensate the actuator nonlinear and frequency dependent characteristics. As the fast tool servo trajectory is synchronized with the spindle rotation, repetitive controller is plugged into the feedback loop to enhance performance of the spindle harmonic trajectory tracking and improve rejection of spindle-generated disturbance.

These methods are implemented on an electromagnetically driven fast tool servo. The experiment results show that the fast tool servo can achieve 10kHz 3dB bandwidth and 160 g acceleration. With the repetitive control, the following errors can be reduced to 7 nm when tracking a 10 μm peak to valley sinusoidal trajectory at 1kHz.

II. Fast Tool Servo Model

Fig. 1 shows the configuration of our electromagnetically driven fast tool servo. Design details about the fast tool servo design can be found in [5]. The backbone of the moving assembly is a carbon fiber tube. On its rear end is attached a disk-shaped armature and the cutting tool tip is installed on the front end. The whole moving assembly is suspended to the FTS frame by two flexures. The armature

is push-pull driven by a pair of circular E-type solenoids in the rear and front sides. The air gaps between the armature and solenoid surfaces are set at $100\mu m$ to allow a $50\mu m$ stroke. The coil windings are implanted into the slots of the solenoids.

A simplified model of the fast tool servo is

$$F = \frac{\mu_0 A}{8}(\frac{Ni_1}{g_0 - X})^2 - \frac{\mu_0 A}{8}(\frac{Ni_2}{g_0 + X})^2, \quad (1)$$

where μ_0 is the permeability, A is the effective area of the armature, g_0 is the air gap at the middle position, N is the turn number of the coils, I_1 and I_2 represent the exciting currents in the front and rear solenoids, and x is the displacement relative to the reference position in the middle of the two solenoids.

For the mechanical system, a simplified model is,

$$\frac{X(s)}{F(s)} = \frac{1}{Ms^2 + Cs + K}, \quad (2)$$

where M is the mass of the moving part, C is the damping from the supporting flexures and the plastic film inserted between air gaps, and K is the stiffness of the flexures.

The position sensing capacitance gauge can be represented by a low pass filter with a pole at 40kHz.

$$\frac{Y(s)}{X(s)} = \frac{1}{\tau_s s + 1}, \quad (3)$$

where Y is the sensor output, and τ_s is the filter time constant associated with the position sensor.

The whole system is controlled by digital computer with sampling time T_s, thus the associated zero-order-hold will bring about $T_s/2$ time delay. The A/D and D/A convertor conversion time and computation time adds up to T_c. Since T_s is selected based on T_c plug the task switching time, they are very close to each other. So the total system time delay will be:

$$T_d = T_c + T_s/2 \simeq \frac{3}{2}T_s. \quad (4)$$

The transfer function for the whole time delay will be:

$$\frac{X_d(s)}{X(s)} = e^{-\frac{3}{2}T_s}, \quad (5)$$

where X_d is the delayed version of position signal X.

III. Dynamic Nonlinear Compensation

The electromagnetically driven actuator is difficult to control in the sense that the actuating force is proportional to the current squared and inversely proportional to the air gap squared. A feedback linearization method was proposed to compensate these nonlinear behavior in [4]. The idea is to compensate the nonlinear model of the actuator using a static inverse model as the compensator, so that all the nonlinear effect cancels out. However, in high frequency operation, the actuating force will decrease with frequency because the magnetic field cannot penetrate the magnetic material as result of the induced eddy current.

To reduce the eddy current induced along the magnetic flux path, in the design phase sintered soft magnetic material is selected for making both the armature and the solenoids. But the eddy current still will appear at high frequency region.

The exist of the eddy current will degrade performance of the linearizing compensator in [4]. To solve this problem, we need a more detailed model than equation (1). The actuator is composed of a pair of solenoid. According to the Maxwell equations we incorporate the eddy current into the model:

$$\overline{H_1} = \frac{Ni_1}{g_0 - X}, \quad \overline{H_2} = \frac{Ni_2}{g_0 + X}, \quad (6)$$

$$H_1 = E(s)\overline{H_1}, \quad H_2 = E(s)\overline{H_2}, \quad (7)$$

$$F = \frac{\mu_0 A}{8}(H_1)^2 - \frac{\mu_0 A}{8}(H_2)^2, \quad (8)$$

where $\overline{H_1}$ and $\overline{H_2}$ represent nominal magnetic field intensity assuming there does not exist any eddy current, H_1 and H_2 are the actual magnetic intensity, $E(s)$ represent the eddy current attenuation effect. Although the eddy current process is governed by partial difference equation, $E(s)$ can be approximated with a half order system with constant -45 degree phase lag at high frequency. By this partition of the actuator model, we can inverse the model part by part as shown in fig. 2. $K_1(x)$ and $K_2(x)$ are the nonlinear position dependent gain between ampere-turn and the nominal magnetic intensity, and the "square" block relates the total magnetic field to the actuating forces. The two inputs of the dynamic compensator F_{D1} and F_{D2} are the desired forces for each solenoid. In order to reduce the requirement on the $\frac{di}{dt}$, a constant force bias F_B is added to the desired actuating force F_D of the whole actuator,

$$F_{D1} = \begin{cases} F_D + F_B & \text{when } \mathrm{F_D} \geq 0 \\ F_B & \text{when } \mathrm{F_D} < 0. \end{cases} \quad (9)$$

$$F_{D2} = \begin{cases} -F_D + F_B & \text{when } \mathrm{F_D} < 0 \\ F_B & \text{when } \mathrm{F_D} \geq 0. \end{cases} \quad (10)$$

Since the biased force will cancel each other, we have

$$F = F_D. \quad (11)$$

According to fig. 2, if $E(s)$ is ignored as constant, then the resulting compensator will be the same as that in [4]. Basically, this dynamic compensation method is feed-forward model based method. The effectiveness is highly dependent on the model accuracy. So in practice, it can partially compensate the nonlinearity of the actuator, but is not expected to linearize the actuator completely.

IV. Loop Compensation

Based on the dynamic nonlinear compensation, the plant can be represented by a linear model:

$$\frac{X_d(s)}{F_D(s)} = \frac{e^{-\frac{3}{2}T_s}}{(Ms^2 + Cs + K)(\tau_s s + 1)}, \quad (12)$$

In order to achieve as high bandwidth as possible, lead compensator is required to ensure enough phase margin. However, the bandwidth of the closed-loop system is limited by the sensor bandwidth and the non-minimum-phase

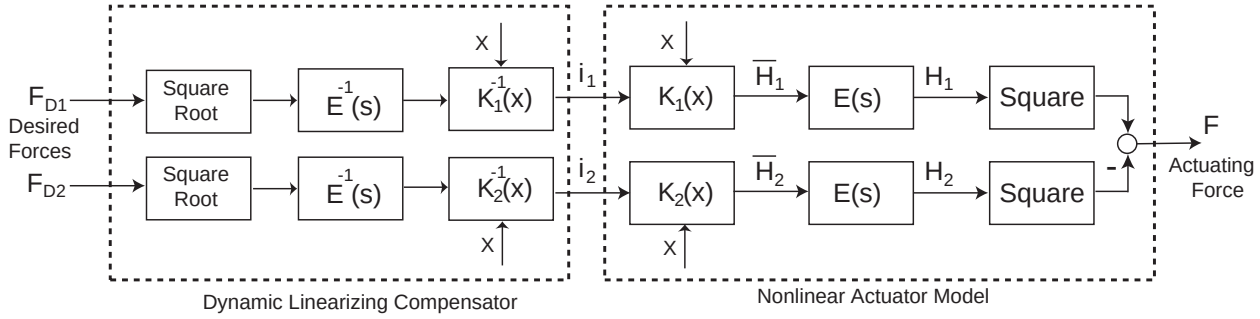

Fig. 2. Dynamic nonlinear compensation block diagram.

element $e^{-\frac{3}{2}T_s s}$. Ideally, if the loop transmission goes across the 0db line with -20db/decade slope, the time delay determine that the cross over frequency ω_c is limited by

$$-\frac{3}{2}T_s\omega_c - \frac{\pi}{2} > -\pi \tag{13}$$

$$\Longrightarrow \omega_c < \frac{1}{6}\omega_s. \tag{14}$$

where ω_s is the sampling frequency. Considering the aliasing effect of the digital controller and the additional phase lag from the sensor dynamics, the intended crossover frequency of the loop transmission is set at 1/20 of the sampling frequency:

$$\omega_c = \frac{1}{20}\omega_s. \tag{15}$$

The phase lag from the time delay at this crossover frequency will be

$$-\frac{3}{2}T_s\omega_c = -\frac{3}{2}\frac{2\pi}{\omega_s}\frac{\omega_s}{20} = -27^\circ. \tag{16}$$

The lead-lag compensator is designed to provide 70 degree phase advance at ω_c. At low frequency region, an integrator is added to increase the controller gain. The compensating controller takes the form of

$$C(s) = K(1 + \frac{K_I}{s})(\frac{\tau_Z s + 1}{\tau_P s + 1}), \tag{17}$$

where K_I is the integrator gain, $\tau_Z = 7/\omega_c$ and $\tau_P = 7\omega_c$ are the time constants for the zero and pole of the lead-lag compensator. K_I is selected to ensure that the system has 30 degree phase margin.

V. Repetitive Control

The trajectory of the fast tool servo is synchronized with the spindle rotation and thus are composed of multiple harmonics at the spindle rotation frequency. Hence most of the trajectory energy are concentrated at multiples of spindle frequency. In order to reduce the tracking error, according to the internal model principle, the resonator models need to be incorporated into the control to enhance the gain of the loop transmission at these frequencies. The repetitive controller are designed as:

$$\sum_{i=1}^{N} \frac{K_i s}{s^2 + \omega_i^2}. \tag{18}$$

where, ω_i is the i-th resonant frequency of the repetitive controller corresponding to the spindle harmonics, K_i is gain of the associated resonator and N is the total number of the implemented resonators. All these resonance frequencies are set below the crossover frequency of the compensated loop in the last section. This repetitive controller is implemented as a plug-in type as shown in fig. 3. In the figure, R is the trajectory input, X is the output position and e is the tracking error signal. The integrator gain is K_0, which is smaller than the controller gain K_I in the last section because additional phase lag will be introduced when plugging these resonator into the loop. Hence, the integer gain needs to be reduced to ensure stability. Actually the integer can also be interpreted as a resonator with resonant frequency of 0:

$$\text{Integrator}: \frac{K_0}{s} = \frac{K_0 s}{s^2 + \omega_0^2}, \tag{19}$$

where $\omega_0 = 0$. From this point of view, all the resonator gains can be tuned to match the integer gain at the cross over frequency.

The integrator in section IV is

$$C_I(s) = 1 + \frac{K_I}{s}. \tag{20}$$

The integrator with repetitive controller plugged in is

$$C_R(s) = 1 + \frac{K_0}{s} + \sum_{i=1}^{N} \frac{K_i s}{s^2 + \omega_i^2}. \tag{21}$$

To ensure controller C_I and controller C_R have the same complex gain at the cross over frequency ω_c of the compensated loop in section IV, we need match their imaginary part at $s = j\omega_c$:

$$-\frac{K_I}{\omega_c} = -\frac{K_0}{\omega_c} + \sum_{i=1}^{N} \frac{K_i \omega_c}{(-\omega_c^2 + \omega_i^2)}, \tag{22}$$

$$\Longrightarrow K_I = K_0 + \sum_{i=1}^{N} \frac{K_i \omega_c^2}{(\omega_c^2 - \omega_i^2)}. \tag{23}$$

When the phase balancing equation of (23) is satisfied, the controller with multiple resonators plugged in will provide the same phase margin and the same cross over frequency as the the controller in section IV, and thus the stability is

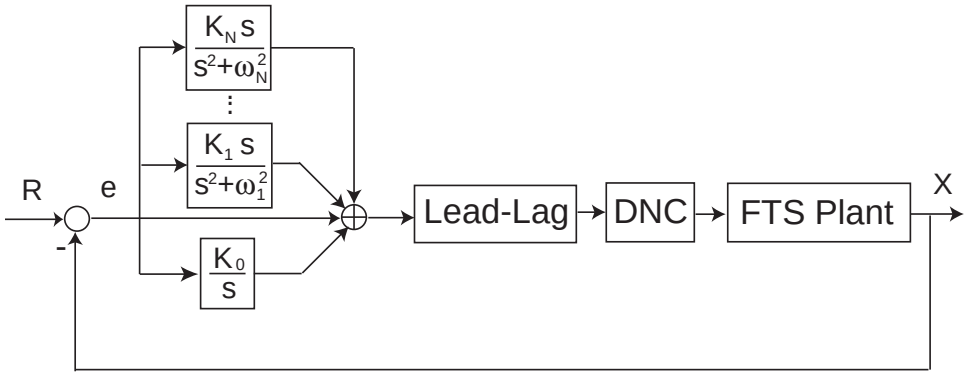

Fig. 3. Block diagram of repetitive controller structure.

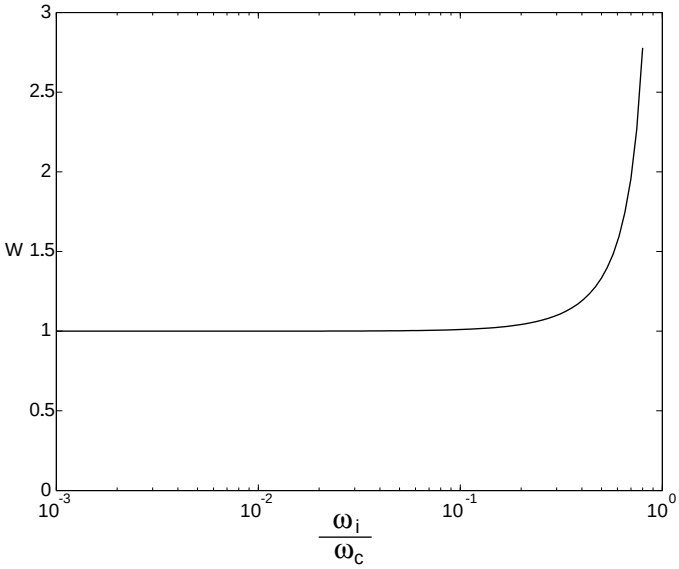

Fig. 4. Resonator gain weighting coefficient as a function of ω_i/ω_c .

guaranteed. According to equation (23), there is a weighting function for the resonator gains

$$W(\omega_i) = \frac{\omega_c^2}{\omega_c^2 - \omega_i^2}. \tag{24}$$

As shown in figure. 4, the horizontal axis is the normalized of the resonant frequency and the vertical axis is the gain weighting coefficient. The higher the resonating frequency ω_i, the more weighting the associated gain and thus more phase lag associated with this resonator. This relation is highly nonlinear. For $\omega_i < 0.5\omega_c$, the gain weighting coefficient W do not change much with the highest value of 1.3 at $\omega_i = 0.5\omega_c$.

Usually all the resonating frequencies are smaller than half of the intended cross over frequency ω_c. In this case, the phase balance equation (23) can be approximated as :

$$K_I = K_0 + \sum_{i=1}^{N} K_i. \tag{25}$$

This means that the resonators can be taken as integrator when selecting their gains. As for how to set the value of

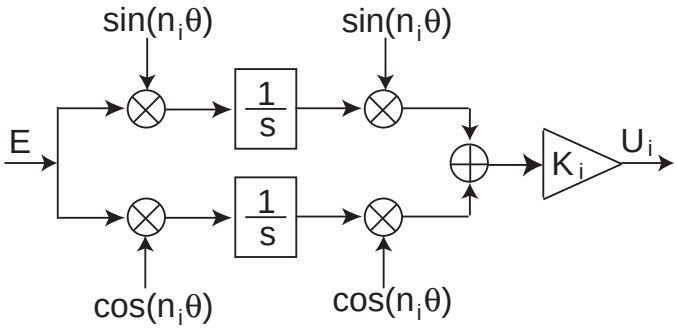

Fig. 5. Resonator implemented in the AFC format.

the resonator gains, this depends on the disturbance force and trajectory amplitudes at various harmonics. A practical way is to set:

$$K_0 = \frac{K_I}{2} \tag{26}$$

$$K_i = \frac{K_I}{2N}, \quad \text{for i} = 1, ..., \text{N}. \tag{27}$$

This is useful especially for varying spindle speed case. When the spindle speed is changing and thus the resonating frequencies of the repetitive control need to change accordingly, K_i can be kept as constant without sacrificing the system stability.

In order to compensate the spindle speed variations, each resonator is implemented in the adaptive feed-forward-cancellation (AFC) format as shown in fig. 5. θ is the spindle rotation angle, and n_i is the order of harmonics of the spindle rotation frequency. If the speed has an angular velocity of Ω, then the $n_i = \omega_i/\Omega$. According to the proof in [6], it can be shown that the relation between e and U_i in Fig. 5 is equivalent to the corresponding resonator block in fig. 3. In this implementation, the resonating frequency is locked to the spindle rotation and thus can effectively reduced the spindle-synchronized trajectory and improve the rejection of the spindle-induced disturbance.

VI. EXPERIMENT AND RESULTS

The controller is implemented using a DSPACE 1103 board, and all the digital controllers are in the discrete domain.

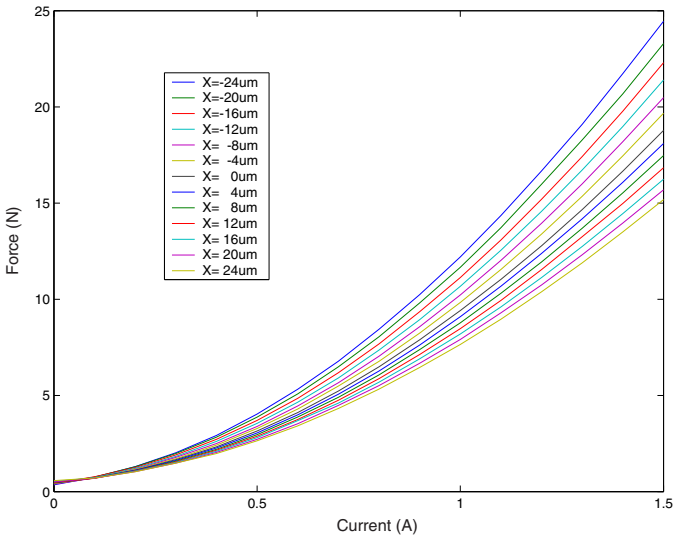

Fig. 6. Actuator Static Characteristics Result.

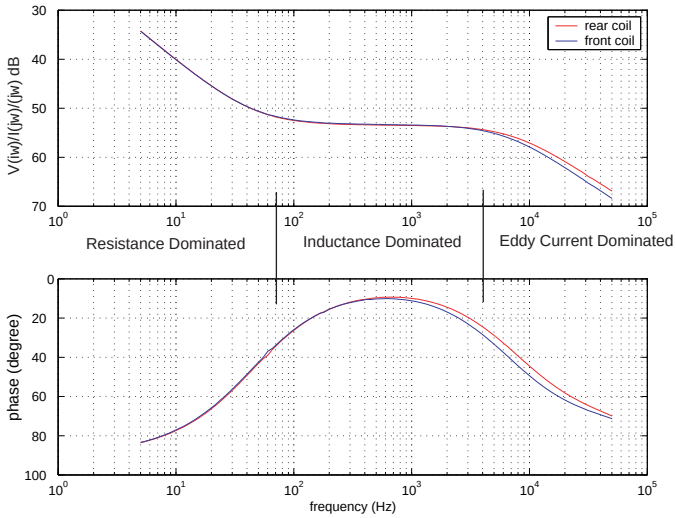

Fig. 7. Actuator eddy current identification result.

A. Plant Identification

In order to implement the dynamic nonlinear compensation method of section III, a static performance test is performed to get the actuator characteristics $K_1(x)$ and $K_2(x)$. The actuating force as a function of armature position and exciting current is shown in fig. 6 for the rear solenoid . From this result, $K_2(x)$ can be fitted out and implemented in the nonlinear compensator.

To compensate the eddy current effect, the $E(s)$ can be extracted by identifying the frequency response from exciting current $I(j\omega)$ to the induced voltage $V(j\omega)$ across the two terminals of the solenoid as shown in fig. 7. The eddy current begin to dominant at 4kHz. A rational transfer function can be fitted to the test result for the frequency rang from 1k to 10kHz and is implemented for the dynamic compensator.

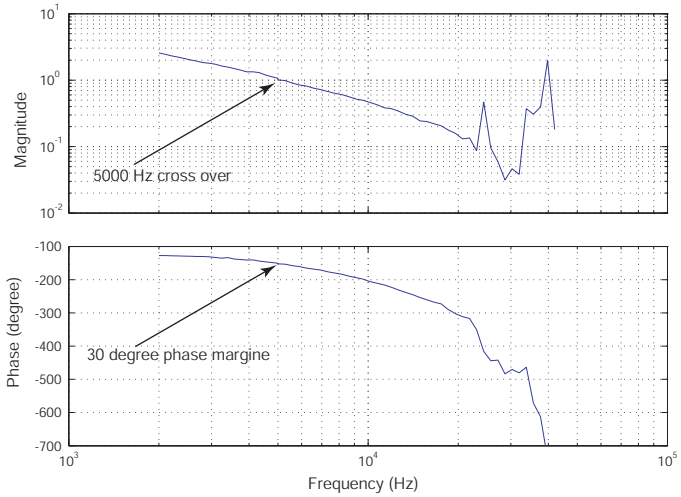

Fig. 8. Frequency response of the compensated loop transmission.

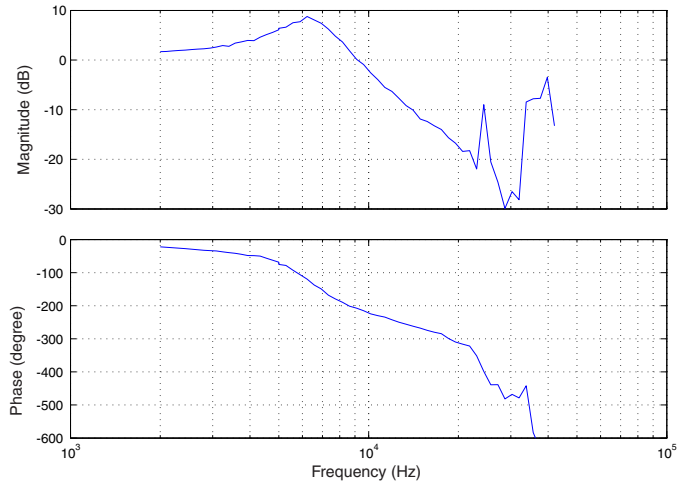

Fig. 9. Frequency response of the closed loop system.

B. Loop Compensation

The compensated loop transmission is shown in fig. 8. The sampling frequency is 100kHz, and the cross over frequency is 5kHz with 30 degree phase margin. The structure resonating peaks above 20kHz will not destabilize the system. The closed loop frequency response is shown in fig. 9. The achieved -3dB bandwidth is 10kHz. Fig. 10 shows a 100nm step response of the closed loop system. For the fixed position command, the regulation root-mean-square(RMS) error is 1.2nm when the spindle is turned off. After the spindle is turned on, the error degrades to 3.5nm RMS because of the PWM noise from the spindle amplifier. The full stroke of 50 μm can be achieved up to 1kHz operation. The maximum acceleration is 160 g when tracking a 9 μm peak-to-valley 3kHz sine wave.

C. Repetitive Control

For the spindle synchronized trajectory, the repetitive controller needs to be plugged into the loop. $10\mu m$ peak-to-valley sine wave trajectory tracking at 1kHz is tested. When no repetitive controller is plugged in, the tracking

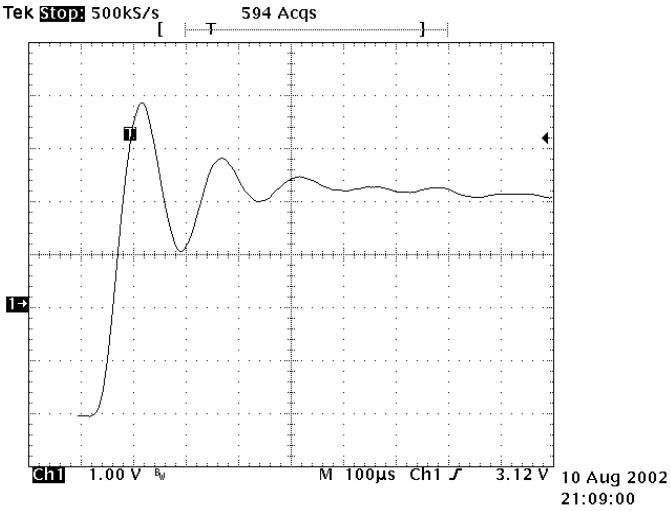

Fig. 10. Step response of the closed loop system.

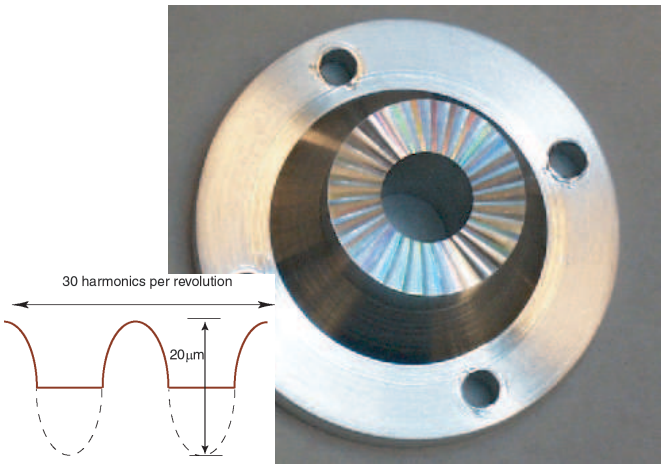

Fig. 11. Diamond Turning Aluminum Surface.

error is 1.048 μm RMS. When a resonator with frequency at 1kHz is applied, the error is 0.0214 μm RMS. The tracking error reduces to 0.0148 μm RMS when a second resonator at 2kHz is further applied and to 0.0073 μm RMS when a third resonator at 3kHz is also added. This shows that the nonlinearity of the actuator and the power amplifier will introduce disturbance forces of second and higher order harmonics, and the repetitive controller with poles at multiple harmonic frequencies can significantly improve the tracking error.

D. Diamond Turning of Aluminum

A cutting experiment is conducted on a Moore diamond turning machine. The same DSPACE 1103 board controls both the X-Z slides of the machine and the FTS. Because the computation ability constraint of the board, a multiple sampling rate system is implemented. The sampling rate for the spindle and X-Z slides controller is 4kHz to ensure that the X-Z slides controls achieve 100Hz bandwidth. As a result, the sampling rate for the FTS controller has to be reduced to 83kHz and the associated cross over frequency is 4kHz for the FTS control loop. As shown in fig. 11, the sinusoidal surface of 30 harmonics per revolution is faced on a piece of aluminum material.

VII. Conclusion

A dynamic nonlinear compensation is introduced to compensate the nonlinearities and frequency dependent characteristics of the electromagnetic actuators. Based on the integrator gain, the plug-in type repetitive controller can be easily designed and implemented. Using these methods, the electromagnetically driven fast tool servo achieves 10kHz bandwidth (-3db) and 7nm error (RMS) for tracking 10μm(peak-to-valley) sine wave at 1kHz.

References

[1] S. R. Patterson, E. B. Magrab, "The design and testing of a fast tool servo for diamond turning", in *Precision Engineering*, Vol. 7, No. 3, pp123-128, 1985.

[2] T. A. Dow, M. H. Miller and P.J. Falter, "Application of a fast tool servo for diamond turning of nonrotationally symmetric surfaces", in *Precision Engineering*, Vol. 13, No. 4, 1991.

[3] Yuichi Okazaki, "Fast tool servo system and its application to three dimensional fine surface figures", in *Proc. of ASPE 1998 annual meeting*.

[4] Subrahmanyan, P.K., Olson, S. M., and Trumper, D.L., "Linearizing Control of Magnetic Suspension Systems", in *IEEE Transactions on Control Systems Technology*, Vol. 5, No. 4, July 1997, pp. 427-438.

[5] Xiaodong Lu and D.L. Trumper, "Electromagnetically Driven Fast Tool Servo", in *Proc. of ASPE 2003 annual meeting*.

[6] Marc Bodson, Alexei Sacks, and Pradeep Khosla, "Harmonic generation in adaptive feedforward cancellation", in *IEEE Transaction on Automatic Control*. Vol. 39, No. 9, Sep 1994.